Supporting Information

Wang et al. 10.1073/pnas.0903554106

SI Text

Fig. S1 shows a representative image (*A*) of a particle diffusing on a lipid tubule and a representative trajectory parallel to the tube extension (*B*).

Fig. S2 shows a typical trajectory of a particle diffusing in entangled F-actin. Comparing trajectories on different time scales, intermittency disappears on long time scales, but exponential tails persist.

Fig. S3 compares mean-square displacement (MSD) normalized by mesh size squared and displacement probability distribution for particles in entangled F-actin.

Fig. S4 shows scatter plots correlating the displacement of representative single particles with their subsequent displacement 4 time steps later (30 × 4 ms).

Fig. S5 presents the displacement transition probability density functions discussed below.

Fig. S6 presents the exchange and persistence time distributions of particles (a = 100 nm) diffusing in entangled F-actin network (ξ = 300 nm). A local event is defined as a displacement distance $>\xi$.

Transition Probability Density Functions. We analyzed the lipid tubule system, where the motion is simply 1D. To inspect correlations between points on a single trajectory, we extracted displacements with time intervals of 30 ms and correlated them with a time delay 4 time steps later (120 ms), the time at which the non-Gaussian parameter (1) of the probability distribution function reaches a maximum. Accompanying a high density of small-amplitude steps, larger steps of broadly dispersed variance are significant as well (Fig. S4*A*). The contrast for a particle diffusing on a tube doped with cholesterol is shown in Fig. S4*B*; the long steps are absent.

Next, on the ensemble level, we calculated transition probability density functions, $P_n(\Delta x',t + n\tau|\Delta x,t)$, where Δx is the 1D displacement in time interval of τ. Fig. S5 *A* and *B* compares the first 2 transition probability functions of beads diffusing in actin networks, and it is obvious to the eye that they also deviate from Gaussian. The shapes of equiprobability are nearly square, corresponding to exponential distribution, not circular, as expected for Gaussian distributions.

In contrast to zero-displacement correlation functions, the weak orientation in P_1 indicates anticorrelation in these displacements. Large positive displacements have more chance to be followed by large negative displacements and vice versa. Interestingly, the symmetry of the pattern still ensures a zero average correlation. However, this weak anticorrelation dies out quickly with time, as one notes from observing that the second-order transition probability, P_2, is essentially isotropic. This observation is also consistent with the picture that particles are hardly trapped under our experimental conditions.

Fig. S5*C* shows that $(P_1^2 - P_2) \approx 0$, illustrating no memory effect on the time scales experimentally available; in other words, these motions are Markovian. Examining the higher-order transition probability functions supports the same conclusion, because $P_1^n \approx P_n$.

Fig. S5*D* shows P_1 for the beads on the lipid tubule system considered in the first section of this article. The qualitative temporal trend and nonspherical shape are evident although these data are noisier because the statistical dataset available for this system is smaller. However, it shows a weak positive correlation of displacement, in accord with the earlier observation of enhanced diffusion.

Membrane Fluctuation Analysis. In the continuum limit and harmonic approximation, membrane undulation in the long time limit is given by

$$\langle(\Delta h)^2\rangle = \frac{k_BT}{\pi\gamma}\ln\left(\frac{L}{\pi}\sqrt{\frac{\gamma}{\kappa}}\right),$$

where $\gamma \approx 10^{-19}$ J, and $\kappa \approx 10^{-4} \sim 10^{-5}$ $J{\cdot}m^2$ are the tension and stiffness of the membrane respectively, L is the tube length, and h is fluctuation amplitude normal to the membrane (2). Inserting known experimental parameters for this system, the estimated amplitude of fluctuations is ≈10 nm, a significant fraction of the particle size. Meanwhile, the relaxation frequency of membrane fluctuation known for hydrodynamic damping in this system,

$$\omega(q) = \frac{\langle z\rangle^3 q^2}{12\eta}(\kappa q^4 + \gamma q^2)$$

corresponds to a time of 5 s, where $q \approx 3 \times 10^5$ m^{-1} is the smallest wave factor considering the particle adsorption, η is the viscosity of bulk water, and $\langle z\rangle \approx 100$ nm is the average lipid tube diameter (3). This pleasing consistency between 2 time scales, 5 s from this calculation and also in the data in Fig. 1*C*, highlights the potential coupling of particle diffusion and membrane fluctuation.

Alternative Random Walk Models. We compare the experimental van Hove functions in the frequency domain by performing the discrete Fourier–Laplace transform of $G_s(x,t) \rightarrow F_s(k,u)$ on these data, with those calculated functions from the continuous time random walk (CTRW) model. Inputting the conjectural jumping length $\psi(k)$ and pausing time $\phi(u)$ distributions into the Montroll–Weiss equation,

$$F_s(k,u) = \frac{1 - \phi(u)}{u}\frac{1}{1 - \psi(k)\phi(u)},$$

best "fittings" are achieved with power-law distributions both for displacements, $\psi(x) \sim x^{-1-\beta}$, and time intermittency, $\phi(\tau) \sim \tau^{-1-\alpha}$, within the range of $0.3 \leq \beta < 0.5$, $2\alpha \approx \beta$ for colloid diffusion on lipid tubule. It is consistent to observe the relation between exponents, $2\alpha \approx \beta$. This satisfies the linear MSD we observed, because according to the CTRW model, this relation corresponds to a complicated spatiotemporal correlation, $\langle\Delta x^2(t)\rangle \sim t^{2\alpha/\beta}$ (4).

Another line of thought considers a dynamic disordered landscape with stochastic potential barriers chosen to have a finite lifetime. As pointed out to us by D. Wu, simulation shows cross-over from Fickian (and Gaussian) behavior, to Fickian and exponential behavior when the barrier lifetime exceeds the mean collision time between particle and barrier.

Einstein's Derivation of Gaussian Statistics Revisited. With these considerations in mind, it is interesting to revisit Einstein's classic derivation of Brownian motion, which forms the basis of the well-known Fokker–Planck equation. It corresponds to a truncation of high-order cumulants in the Kramers–Moyal expansion of the Markovian master equation (5), which leads to recovering Fick's diffusion equation. Physically, those high-

order terms connect to the nonlinear dissipations. This truncation supposes that the mass and the momentum of the surrounding particles are infinitesimally small (5). Naively, it is appropriate to question its legitimacy in complex fluids such as those studied experimentally in this article, where the environment is massive in both mass and momentum. But it is difficult to make progress with this argument. Although there is continuous theoretical effort to involve higher-order terms (6), this is a demanding task for lack of appropriate mathematical tools and the common belief that high-order corrections are of little importance. This is perhaps appropriate because of the paucity of relevant data with which to compare. Computer simulations have for decades often measured the nonzero non-Gaussian parameters in various diffusion processes (7, 8). This essentially reflects high-order cumulants of the displacement probability, but the full distribution in general was not explicitly explored.

Persistence and Exchange Time Distributions. These times are defined according to Chandler and Garrahan (9–11). In brief, consider a particle i, initially at $t_0 = 0$ observed at position $r_i(0)$. The persistence time t_1 for a cutoff distance d is specified by the first time that particle i has moved far enough that $|r_i(t_1) - r_i(0)| \geq d$. Exchange times $t_n - t_{n-1}$ for $n > 1$, require the recursive determination t_n from t_{n-1}, with t_n defined as the first time that particle i has moved far enough so that $|r_i(t_n) - r_i(t_{n-1})| \geq d$. For a given threshold distance d, distributions of exchange and persistence times can be obtained by ensemble averaging over all trajectories.

When computing these quantities, care must be taken to avoid biasing the data because of the finite time extent of the trajectories. Trivially, the probability of observing a time interval greater than the total time span of the trajectory is zero, placing an absolute upper bound on the window of times we can measure. More importantly, when computing exchange times, for each subsequent t_n, the time remaining till the end of the trajectory decreases, continually narrowing the window over which our relative probabilities are accurate. The decreasing window results in a noticeable bias to the data, increasing the relative probability of shorter time intervals. Fortunately, this problem can be circumvented with minimal difficulty by simply reserving a portion at the end of each trajectory during which measured displacements are allowed to terminate but not to start. In so doing, bias will be limited to time intervals greater than the extent of the reserved portion, whereas the relative probabilities will be accurate for all time intervals less than this extent. Because of largely discarding a portion of the trajectory, a tradeoff therefore exists between the size of the window of accurately observable times and the precision of the observations. For all results presented here, time intervals were selected to avoid any bias in the figures.

Further improvement was obtained by increasing the sampling of the trajectories; in effect, the initial time t_0 was arbitrary, and similar analysis can be applied for $t_0 = 1, 2$, etc. In practice, although significantly increasing the data available, special consideration must be applied when implementing increased sampling. In contrast to ensemble averaged trajectories, oversampled trajectories are not fully statistically independent, so when calculating the precision, careful consideration must be given to the number of independent degrees of freedom. Although not exactly analogous, a more thorough explanation of this issue is provided by Valentine and Weitz (12), who determined the number of independent degrees of freedom obtained by oversampling of trajectories when computing the mean-squared displacement. To determine precise error bars for the persistence and exchange distributions, similar analysis would need to be used to determine the degree of statistical independence for these calculations. A simpler estimate of the error bars corresponds to the roughness of the curves of the distributions.

Because the roughness of these curves in Fig. 5 and Fig. S6 is minimal compared with the qualitative differences observed in this article, although not precisely calculated, the error bars for our measurements would be insufficient to alter our qualitative observations.

Details Regarding Materials and Methods. ***Colloidal beads on phospholipid bilayer tubes.*** Tubular lipid vesicles were produced by drying a suspension of liposomes composed of dilauroylphosphatidylcholine (DLPC; Avanti Polar Liquids) on a clean glass slide, followed by prehydration in water vapor and then hydration in water or buffer. Tubes form with diameters ranging from 100 nm to 1 μm and lengths of several hundred microns. Carboxylate-modified fluorescent colloidal polystyrene spheres with diameter $\sigma = 100$ nm (Interfacial Dynamics) were added after the phospholipid tubes relaxed.

Colloidal beads in entangled actin suspensions. Lyophilized G-actin (rabbit skeletal muscle; Cytoskeleton) was reconstituted in fresh G-buffer (5 mM Tris [Tris(hydroxymethyl)aminomethane] at pH 8.0, supplemented with 0.2 mM $CaCl_2$, 1 mM ATP, and 0.2 mM DTT and 0.01% NaN_3) at 4 °C and used within 7 days of reconstitution. G-actin was polymerized into F-actin by the addition of salt (100 mM KCl, 2 mM $MgCl_2$), in the presence of gelsolin (human plasma; Cytoskeleton) to control the length of the filaments (13). In other control experiments, the ATP concentration was varied to show no dependence of observations on ATP level (0.1–1 mM), thus confirming that treadmilling, whose time scale is hours (14), is negligible for the duration of these experiments.

Fluorescent tracer particles, carboxylate modified colloidal polystyrene nanospheres (Molecular Probes), were coated with BSA (Sigma–Aldrich), a widely used blocking protein (15), to preclude nonspecific adsorption. The extra BSA was removed from the solution by repeated centrifugation (25,000 $\times$ g for 30 min) and washing. The possible aggregates were filtered out by passing the modified particles through PVDF membranes (Millipore) with pore size cutting off single nanospheres. Modifying the surface has only a small effect on the particle motion.

The probes were added into G-actin solutions at concentration $\approx 10^{-15}$ M immediately before polymerization. After mixing and polymerization, the samples were stabilized on the microscope stage for at least 4 h. We focused $\approx$100 μm into the sample to avoid wall effects. To reduce the noise in displacement probability distribution, $\approx$100 particles were imaged in the field of view, and $\approx$50 movies were taken from 3–5 samples for each condition.

Single-particle tracking. The samples were imaged by using a homebuilt setup for epifluorescence microscopy with a diode-pumped Nd/YAG laser (CrystaLaser) excitation source (14). The laser was focused to the back focal point of an air objective (LD Neofluor 63×, N.A. = 0.75), causing the beam out of the objective to be parallel and homogeneous. Fluorescence excited was collected through the objective and detected by a back-illuminated electron-multiplying CCD camera (Andor iXon DV-897 BV). The total system magnification of the CCD was 100 nm/pixel. Fluorescence images were collected typically at the speed of 20 frames per second for 500 s. The video images were converted into digital format and analyzed by using single-particle tracking programs, locating the center of each particle in each frame and then stringing these positions together to form trajectories by using software written in-house (16, 17). The accuracy was $\approx$20 nm (17).

For the case of particles diffusing on lipid tubules, before the movies can be analyzed by using standard particle tracking algorithms, the fluorescent contribution of the tubes must be subtracted. We exploited their effectively constant contribution.

For the majority of the time, the intensity of a pixel reflected the background value with a small noise component. Thus, if we average the value of a pixel over all times after discarding the brightest quarter, we obtain an almost perfect background image. Some distortion persists because the average value at those locations where a particle was never present will be slightly too low, but this deviation is minimal and acceptable because this random noise is trivial compared with tube fluorescence. This has the beneficial side effect of excluding fixed particles from consideration. Finally, the trajectories are projected to the axis parallel to the extending direction of the tubes for further statistical analysis.

1. Odagaki T, Hiwatari Y (1991) Gaussian-to-non-Gaussian transition in supercooled liquids. *Phys Rev A* 43:1103–1106.
2. Daillant J, et al. (2005) Structure and fluctuations of a single floating lipid bilayer. *Proc Natl Acad Sci USA* 102:11639–11644.
3. Kaizuka Y, Groves JT (2006) Hydrodynamic damping of membrane thermal fluctuations near surfaces imaged by fluorescence interference microscopy. *Phys Rev Lett* 96:118201.
4. Baskin E, Iomin A (2004) Superdiffusion on a comb structure. *Phys Rev Lett* 93: 120603.
5. Risken H (1989) *The Fokker–Planck Equation* (Springer, Berlin).
6. van Kampen NG (1981) *Stochastic Process in Physics and Chemistry* (North-Holland, Amsterdam).
7. Kob W, Donati C, Plimpton SJ, Poole PH, Glotzer SC (1997) Dynamical heterogeneities in a supercooled Lennard–Jones liquid. *Phys Rev Lett* 79:2827–2830.
8. Odagaki T, Hiwatari Y (1991) Gaussian-to-non-Gaussian transition in supercooled liquids. *Phys Rev A* 43:1103–1106.
9. Hedges LO, Maibaum L, Chandler D, Garrahan JP (2007) Decoupling of exchange and persistence times in atomistic models of glass formers. *J Chem Phys* 127:211101.
10. Chaudhuri P, Berthier L, Kob W (2007) Universal nature of particle displacements close to glass and jamming transitions. *Phys Rev Lett* 99:060604.
11. Berthier L, Chandler D, Garranhan JP (2005) Length scale for onset of Fickian diffusion in supercooled liquids. *Europhys Lett* 69:320–326.
12. Valentine MT, et al. (2001) Investigating the microenvironments of inhomogeneous soft materials with multiple particle tracking. *Phys Rev E* 64:061506.
13. Janmey PA, Peetermans J, Zaner KS, Stossel TP, Tanaka T (1986) Structure and mobility of actin filaments as measured by quasielastic light scattering, viscometry, and electron microscopy. *J Biol Chem* 261:8357–8362.
14. Sheterline P, Clayton J, Sparrow JC (1998) *Actin* (Oxford Univ Press, New York), 4th Ed.
15. Valentine MT, et al. (2004) Colloid surface chemistry critically affects multiple particle tracking measurements of biomaterials. *Biophys J* 86:4004–4014.
16. Anthony SM, Zhang L, Granick S (2006) Methods to track single-molecule trajectories. *Langmuir* 22:5266–5272.
17. Anthony SM, Granick S (2009) Image analysis with rapid and accurate 2D Gaussian fitting. *Langmuir* 25:8152–8160.

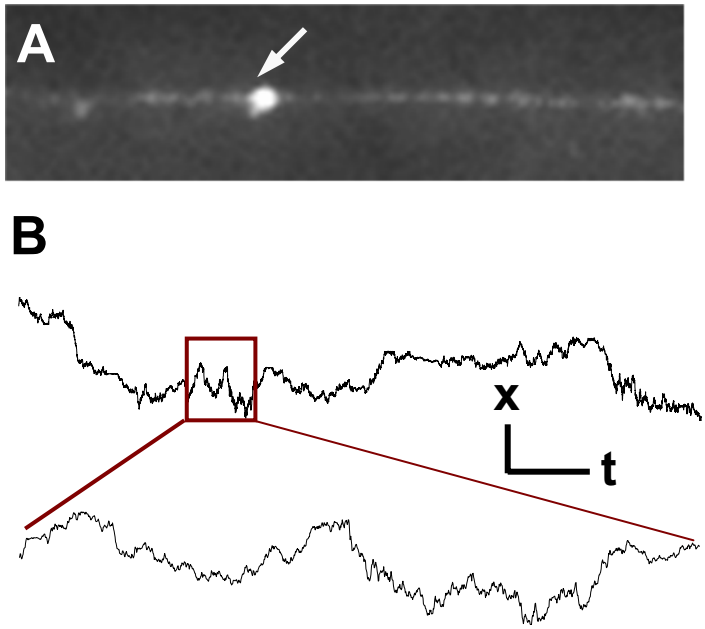

Fig. S1. (*A*) Representative image of a particle diffusing on a lipid tubule. The arrow shows the particle. The image size is 5 × 20 μm. Image analysis allows us to measure relative displacements of 20 nm. (*B*) Representative trajectory parallel to the tube extension. The coordinate scales in the upper trace are 10 σ and 50 s. In the lower trace, the scales are 4.5 σ and 5 s. Each time step is 30 ms.

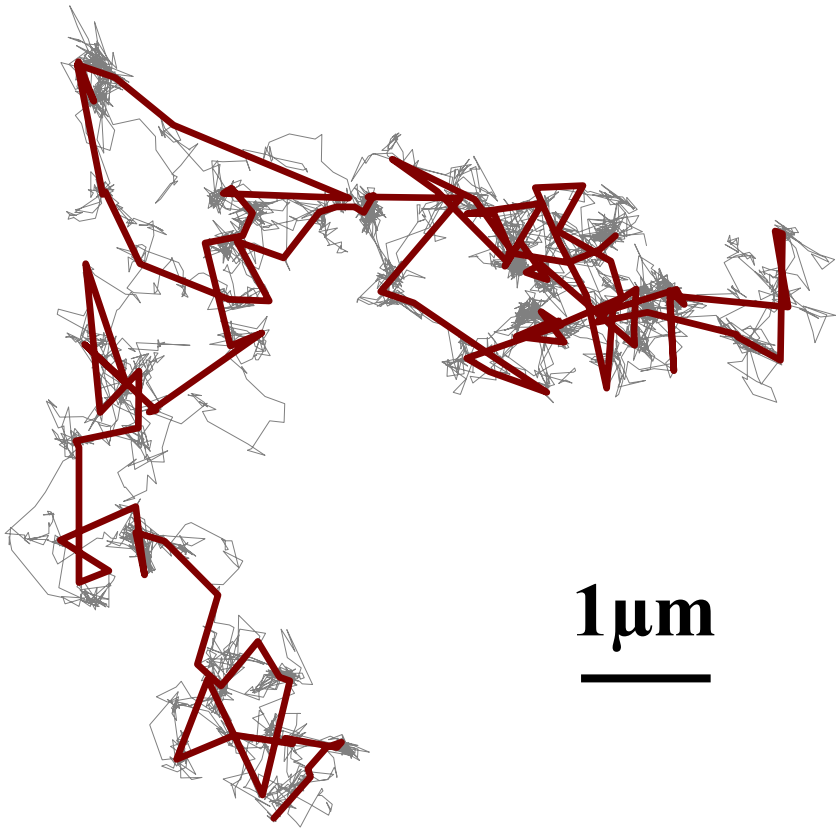

Fig. S2. A typical trajectory of particle ($a = 100$ nm) diffusing in entangled F-actin ($\xi = 300$ nm) projected onto the x–y plane with 50 ms between frames (gray) or 2 s between frames (red), measured for 250 s. The eye distinguishes local vibrations and long jumps (gray line); for this sampling time, motion is determined to be subdiffusive, a pattern familiar in colloidal systems and commonly attributed to ''caging.'' Increasing the time period of temporal sampling by a factor of 40 (red line) makes the long jumps more obvious to the eye, corresponding to reversion of motion to Fickian.

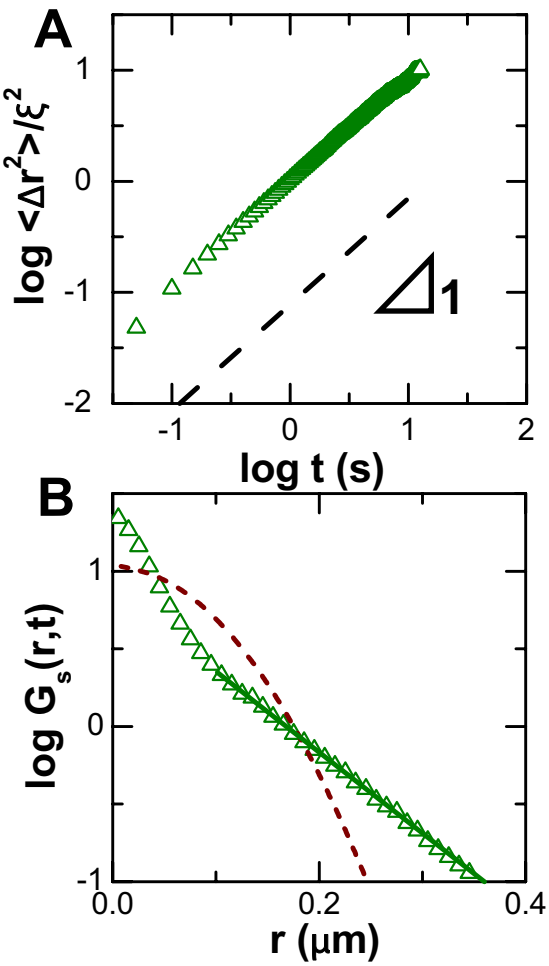

Fig. S3. Comparison of mean-square displacement (MSD) normalized by mesh size squared, plotted against time t on a log–log scale for particles in entangled F-actin at conditions of $a = 100$ nm, $\xi = 450$ nm. MSD, shown in *A* has slope of unity. The corresponding displacement probability distribution $G_s(r,t)$ is plotted logarithmically against linear displacement for delay time of 0.1 s in *B*. Here, $G_s(r,t)$ can be fitted with a combination of a Gaussian function at small displacement and an exponential function at large displacement, indicated by the solid line. The dashed line in *A* is MSD constructed according to the central Gaussian part in displacement distribution. The dashed line in *B* shows a Gaussian distribution with the same diffusion coefficient as for the measurements in *A*.

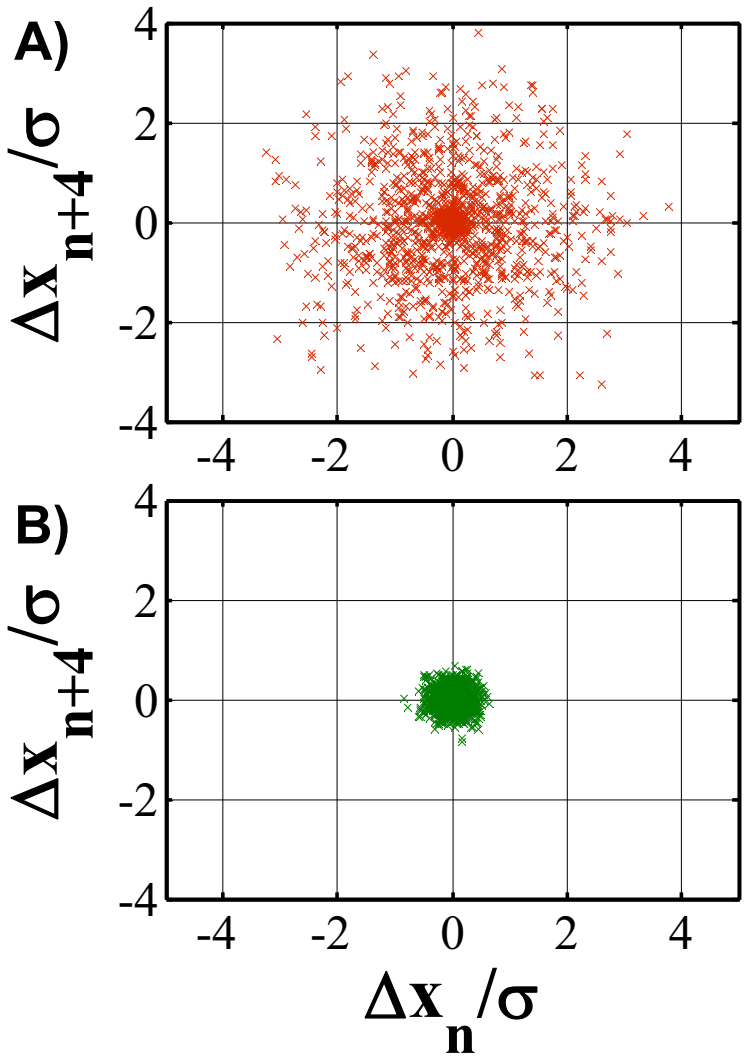

Fig. S4. Scatter plots correlating the displacement of representative single particles with their subsequent displacement 4 time steps later (30 × 4 ms); this is the time at which the non-Gaussian parameter of the probability distribution function reaches a maximum. (*A*) For particles diffusing on tubes of pure DLPC, the diffuse scatter of displacements indicates that the particles move persistently but with dispersive variance. (*B*) Particles diffusing on tubes of DLPC containing 40% cholesterol show no such heterogeneity.

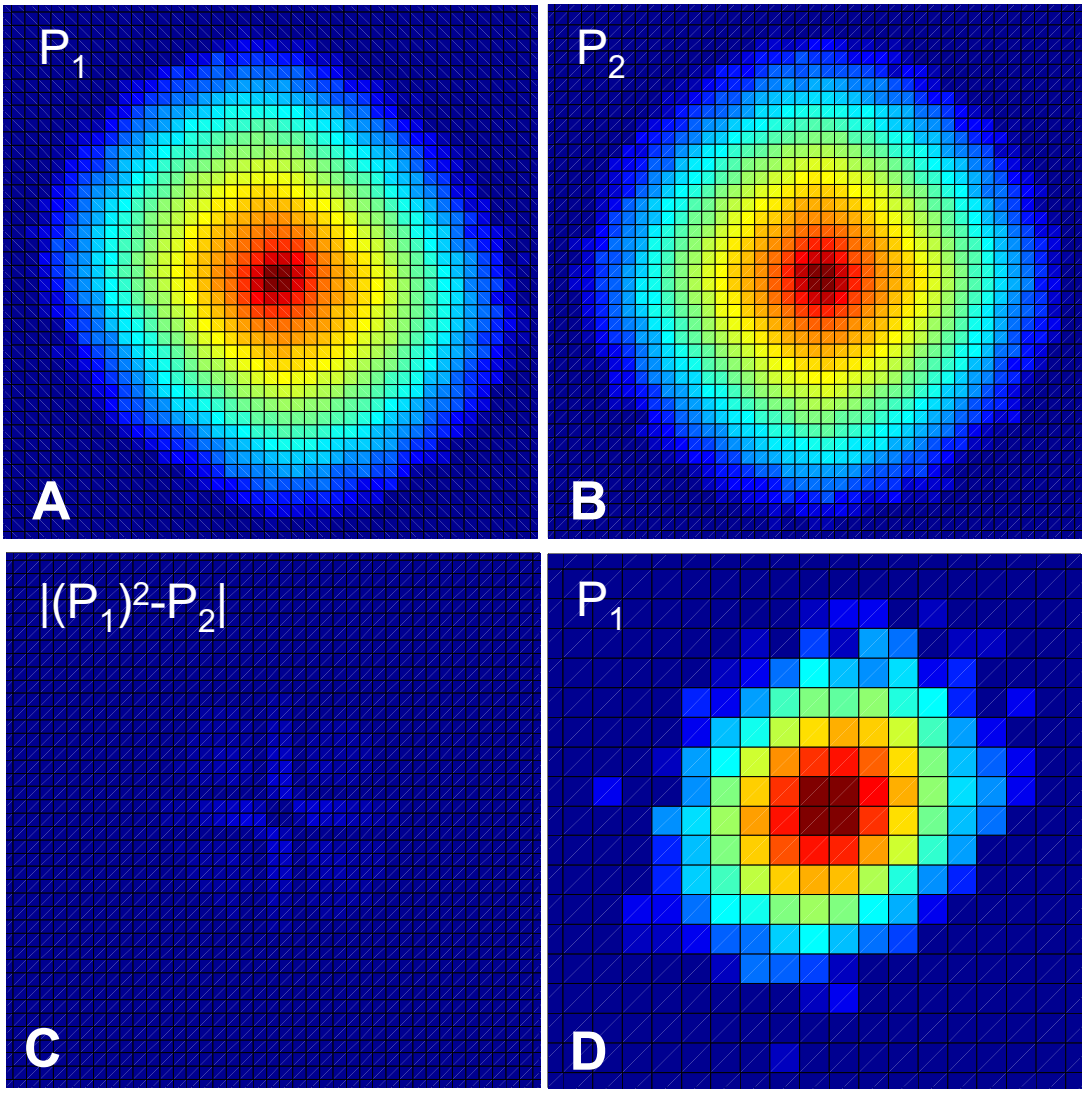

Fig. S5. Displacement transition probability density functions, $P_n(\Delta x', t + n\tau | \Delta x, t)$, where Δx is the 1D displacement in time interval of τ. The color is coded as the logarithmic probability density covering 3 orders of magnitudes. *A*, *B*, and *C* show the P_1, P_2, and $|(P_1)^2 - P_2|$, respectively, of particles ($a = 50$ nm) diffusing in entangled actin network ($\xi = 300$ nm), with $\tau = 50$ ms. The binning width is 50 nm. Here, $P_n(0, t + n\tau | 0, t)$ is located at the centers of the plots; *D* shows P_1 of particles ($\sigma = 100$ nm) diffusing on a lipid tubule, with $\tau = 30$ ms. The binning width is 100 nm.

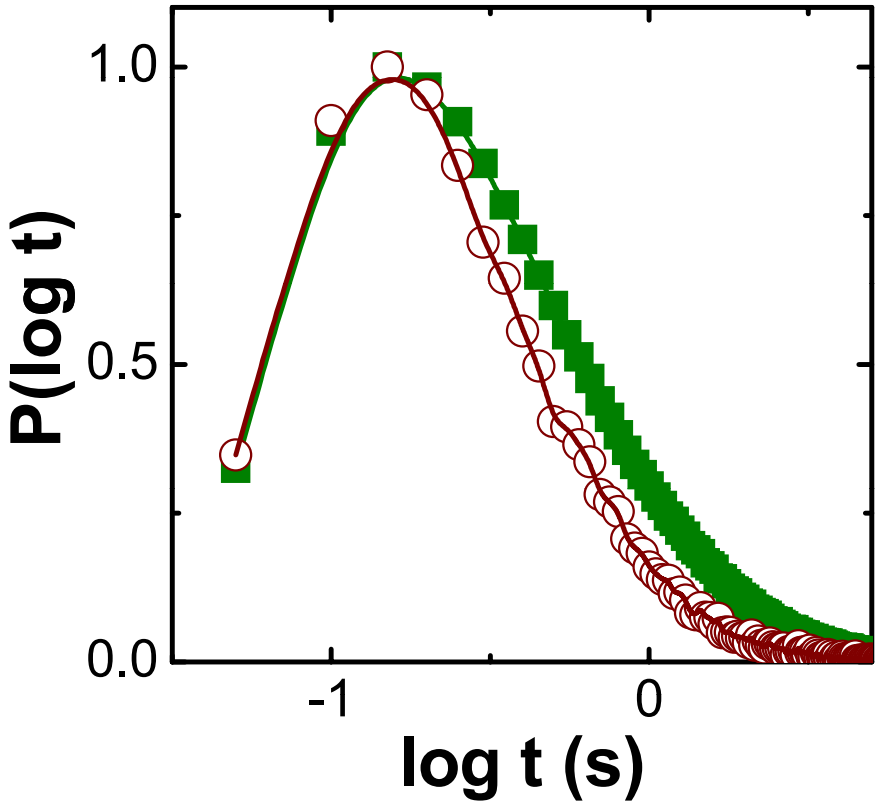

Fig. S6. Exchange (circles) and persistence (squares) time distributions of particles (a = 100 nm) diffusing in entangled F-actin network (ξ = 300 nm). A local event is defined as a displacement distance $>\xi$.